CHEMMEDCHEM

CHEMISTRY ENABLING DRUG DISCOVERY

Accepted Article

Title: Design and synthesis of DNA-interactive β-carboline-oxindole hybrids as cytotoxic and apoptosis inducing agents

Authors: Shankaraiah Nagula, Ramya Tokala, Sowjanya Thatikonda, Sravani Sana, Usha Sree Vanteddu, and Chandraiah Godugu

To be cited as: *ChemMedChem* 10.1002/cmdc.201800402

Link to VoR: http://dx.doi.org/10.1002/cmdc.201800402

A Journal of

ChemPubSoc Europe

WILEY-VCH

www.chemmedchem.org

Design and synthesis of DNA-interactive β-carboline-oxindole hybrids as cytotoxic and apoptosis inducing agents

Ramya Tokala,[a] Sowjanya Thatikonda,[b] Usha Sree Vanteddu,[a] Sravani Sana,[a] Chandraiah Godugu,[b]* Nagula Shankaraiah[a]*

Abstract: A new series of (*E*)-3-((1-aryl-9*H*-pyrido[3,4-*b*]indol-3-yl)methylene)indolin-2-one hybrids have been synthesized and evaluated for their *in vitro* cytotoxic activity against a panel of selected human cancer cell lines namely, HCT-15, HCT-116, A549, NCI-H460, MCF-7 including HFL. Among the tested compounds, (E)-1-benzyl-5-bromo-3-((1-(2,5-dimethoxyphenyl)-9*H*-pyrido[3,4-*b*]indol-3-yl)methylene)indolin-2-one (Compound **10s**) showed potent cytotoxicity against HCT-15 cancer cells with an IC_{50} value of 1.43 ± 0.26 μM and GI_{50} value of 0.89 ± 0.06 μM. Notably, induction of apoptosis by **10s** on HCT-15 cell line was characterized by using different staining techniques such as acridine orange/ethidium bromide (AO/EB) and DAPI. Further, to understand the mechanism of anticancer effects various assays such as annexin V-FITC/PI, DCFDA, and JC-1were performed. The flow cytometric analysis revealed that compound **10s** arrests the HCT-15 cancer cells at the G0/G1 phase of cell cycle. Additionally, western blot analysis indicated, the treatment of **10s** on HCT-15 cancer cells led to decreased expression of anti-apoptotic Bcl-2 and increased protein expression of both pro-apoptotic Bax and caspase-3, 8, 9 and cleaved PARP with reference to actin. Next, clonogenic assay revealed the inhibition of colony formation in HCT-15 cancer cells by **10s**, in a dose-dependent manner. Moreover, the compounds when tested on normal human lung cells (HFL) were observed to be safer with low toxicity profile. In addition, viscosity and molecular docking studies showed that compound **10s** having typical intercalation with DNA.

Introduction

Cancer is growing as the leading cause of mortality and accounts for the major morbidity worldwide.[1] According to World Health Organisation (WHO), cancer is liable for 8.8 million deaths in year 2015 and was predicted to rise over 13.1 million by 2030.[2] It is characterized by the growth of cells beyond their boundaries and invasion of tissues making it dreadful of all the diseases. Despite of the chemotherapeutic agents being currently available, the tolerance, resistance and the unwanted toxic effects towards chemotherapy demands for necessity in the development of new anticancer agents. DNA, till date is a major target in cancer therapy due to its vital role in cell division (replication), maintenance (transcription), and new chemical entities (NCEs) targeting DNA can be remarkable representatives as potent chemotherapeutics.[3,4] Beyond this, evading apoptosis stands out as emerging hallmark of cancer[5] and as a result the compounds inducing apoptosis can evolve as potential anticancer agents. Considering these facts, the search towards the development of novel compounds that would target DNA and induce apoptosis plays an effective role in cancer therapy.

The β-carboline alkaloids were naturally obtained from seeds of *Peganum harmala* (*Zygophillaceae*) and they contain tricyclic pyrido[3,4-*b*] indole ring system.[6] These alkaloids were known to exert their pharmacological and medicinal properties[7] like anxiolytic (Abecarnil), anti-alzheimer, anticonvulsant, antifungal, antimicrobial, antiplasmodial, antiviral, antiplatelet, and antimutagenic effects along with antitumor activity.[8] This class of heterocycles was known to exert their activity through variable mechanisms such as i) interaction with DNA[9], ii) action on CDK's,[10-16] and iii) inhibition of topoisomerase I & II.[17] Apart from these, a mechanism of photocleavage of DNA has also been reported.[18] Recently, a harmine (**A, Figure 1**) derivative CM16 (**B, Figure 1**) was reported to inhibit translation step of protein synthesis.[19] 3-Formyl-9*H*-β-carboline and diversity at C1-position was reported as an aldo-X bifunctional building block (AXB3s) by target-oriented synthesis.[20] DNA targeting anticancer agents show their efficacy by recognition and binding to DNA through intercalation via G-C base pairs such examples are Mana-Hox (**C, Figure 1**), doxorubicin (Hodgkin's sarcoma) and dactinomycin (Ewing's sarcoma).[21]

On the other hand, 2-oxindole is a well-known "privileged heterocyclic scaffold"[22] and displays versatile actions both in terms of biology and pharmacology. Oxindoles show their potent anticancer activity through inhibition of diverse kinases like cyclin-dependent kinase (CDKs) and tyrosine kinases.[23] Oxindole containing marketed drug sunitinib (**D, Figure 1**) shows multi-targeted kinase inhibition and is in clinical use for the treatment of renal carcinoma and imatinib-resistant gastrointestinal stromal tumour (GIST).[24] This is the first cancer drug that has been approved simultaneously for two indications. Later, investigational new drug candidates such as SU5416 (**E, Figure 1**) and SU6668 were also evaluated for their cytotoxic potential against different tumors. FDA approved sunitinib and investigational drug candidates like SU5416, SU6668 have been synthesized based on C3 modification of oxindole moiety. Moreover, Kamal and co-workers have also reported imidazopyridine-oxindole conjugates as potential cytotoxic agents against 50 cancer cell lines.[25a] Hence, the C3 functionalization of oxindole acts as an attractive site for the development of new potent molecules along with structural modifications at C5 and N1 positions. [25, 22]

[a] R. Tokala, U. S. Vanteddu, S. Sana, Dr. N. Shankaraiah
Department of Medicinal Chemistry
National Institute of Pharmaceutical Education and Research (NIPER)
Hyderabad 500 037, India
E-mail: shankar@niperhyd.ac.in
[b] S. Thatikonda, Dr. C. Godugu
Department of Regulatory Toxicology
National Institute of Pharmaceutical Education and Research (NIPER)
Hyderabad 500 037, India
E-mail: chandra@niperhyd.ac.in

Supporting information for this article is given via a link at the end of the document.

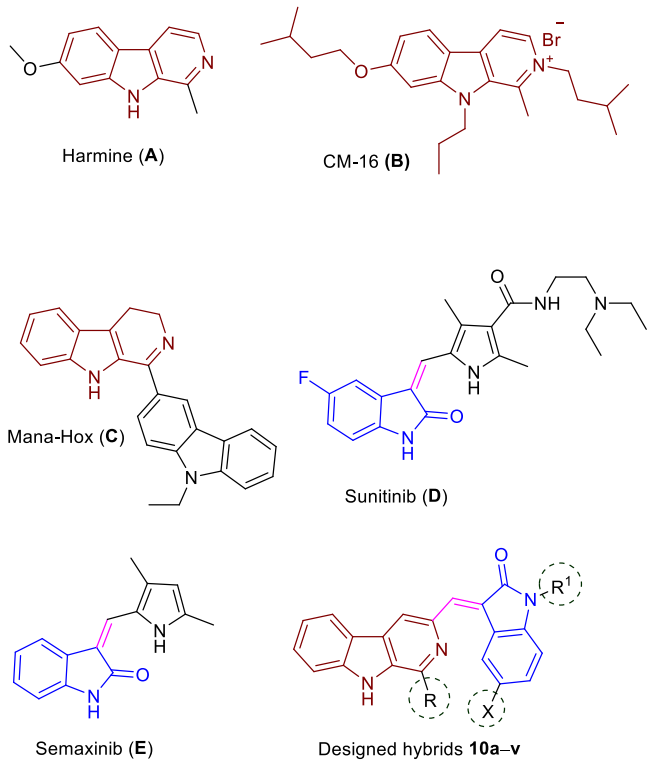

Figure 1. Structures of biologically active β-carbolines (**A**–**C**), oxindoles (**D** & **E**), and newly designed hybrids **10a**–**v**.

Molecular hybridization is a tool in favor of adjoining two distinct biologically important chemical entities covalently into one novel hybrid towards the discovery of desired potent hybrid molecules.[22] Moreover, hybridization of such two dissimilar scaffolds with a different mechanism of actions might result in synergistic effects with improved efficacy and also minimize the off-target effects. This pharmacophoric alteration presents in the hybrids with different or dual modes of action possessing high affinity and selectivity.[26] In this regard, considering the therapeutic importance of formyl-9*H*-β-carboline and 2-oxindoles towards our venture for the synthesis of potent anticancer agents, herein we have designed hybrids of these two pharmacophores with structural diversity by employing Knoevenagel condensation (**Figure 2**).

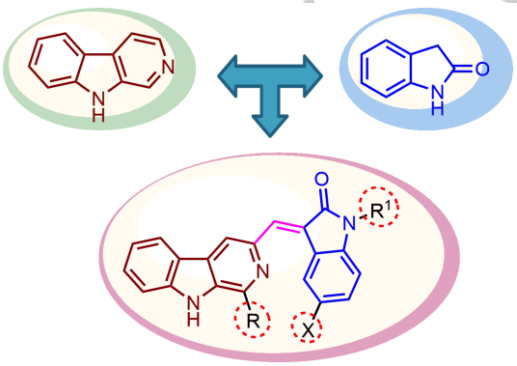

Figure 2. Molecular hybridization between β-carbolines and 2-oxindoles.

Results and Discussion

Chemistry

The β-carboline-linked oxindole hybrids **10a**–**v** were synthesized in a convergent approach by utilizing the multifaceted Knoevenagel condensation reaction between variously substituted oxindoles **3a**–**d** and 1-aryl-9*H*-pyrido[3,4-*b*]indole-3-carbaldehydes **9a**–**g** as depicted in **Scheme 1**. The 2-oxindoles **3a**–**d** were synthesized according to the previous reports.[22] The substituted isatins **1a**–**c** were N-alkylated using different alkylating agents in the presence of base followed by subsequent Wolff-Kishner reduction with hydrazine hydrate in reflux conditions to furnish the corresponding 2-oxindoles **3a**–**d** in overall good yields.[27, 28] Next, another component, 1-aryl-9*H*-pyrido[3,4-*b*]indole-3-carbaldehydes **9a**–**g** were synthesized according to the reported methods.[9b, 29] The commercially available L-tryptophan **4** was esterified using thionyl chloride in methanol solvent. Thus obtained, L-tryptophan ester **5** was subjected to Pictet-Spengler reaction with different aldehydes employing a catalytic amount of TFA. The diastereomers **6a**–**g** thus obtained was aromatized using $KMnO_4$ followed by reduction of ester functionality with $LiAlH_4$ provided the corresponding alcohols **8a**–**g**. Then, the alcohols were subsequently oxidized into their corresponding aldehydes **9a**–**g** by activated MnO_2. Finally, the desired hybrids **10a**–**v** were accomplished by employing Knoevenagel condensation reaction between **9a**–**g** and **3a**–**d** with a catalytic amount of piperidine as a base. It is important to note that all the final compounds were obtained and characterized as single isomers and solids by simple filtration.

One of the representative compounds **10a** was confirmed using ^{1}H NMR by the appearance of a characteristic singlet at *δ* 7.82 ppm which accounts the proton after condensation reaction. The two signals at *δ* 11.92 and 10.55 ppm account for -NH-protons on oxindole and 9*H*-indolic proton of β-carboline. All the remaining protons lie in the range 6.77-9.35 ppm of the aromatic region. Next, the analysis of ^{13}C NMR depicts the presence of carbonyl carbon of oxindole at *δ* 170.3 ppm. All other aromatic carbons of **10a** were in the range of aromatic region *δ* 79.6-143.5 ppm. Similarly, the other derivatives **10b**–**v** were well matched with their respective structures (^{1}H, ^{13}C NMR & FT-IR).

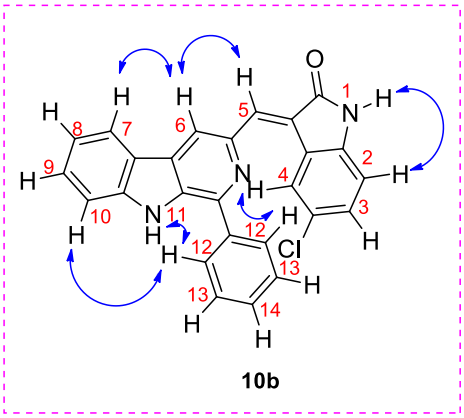

Figure 3. Determination of configuration for representative compound **10b** by NOE analysis.

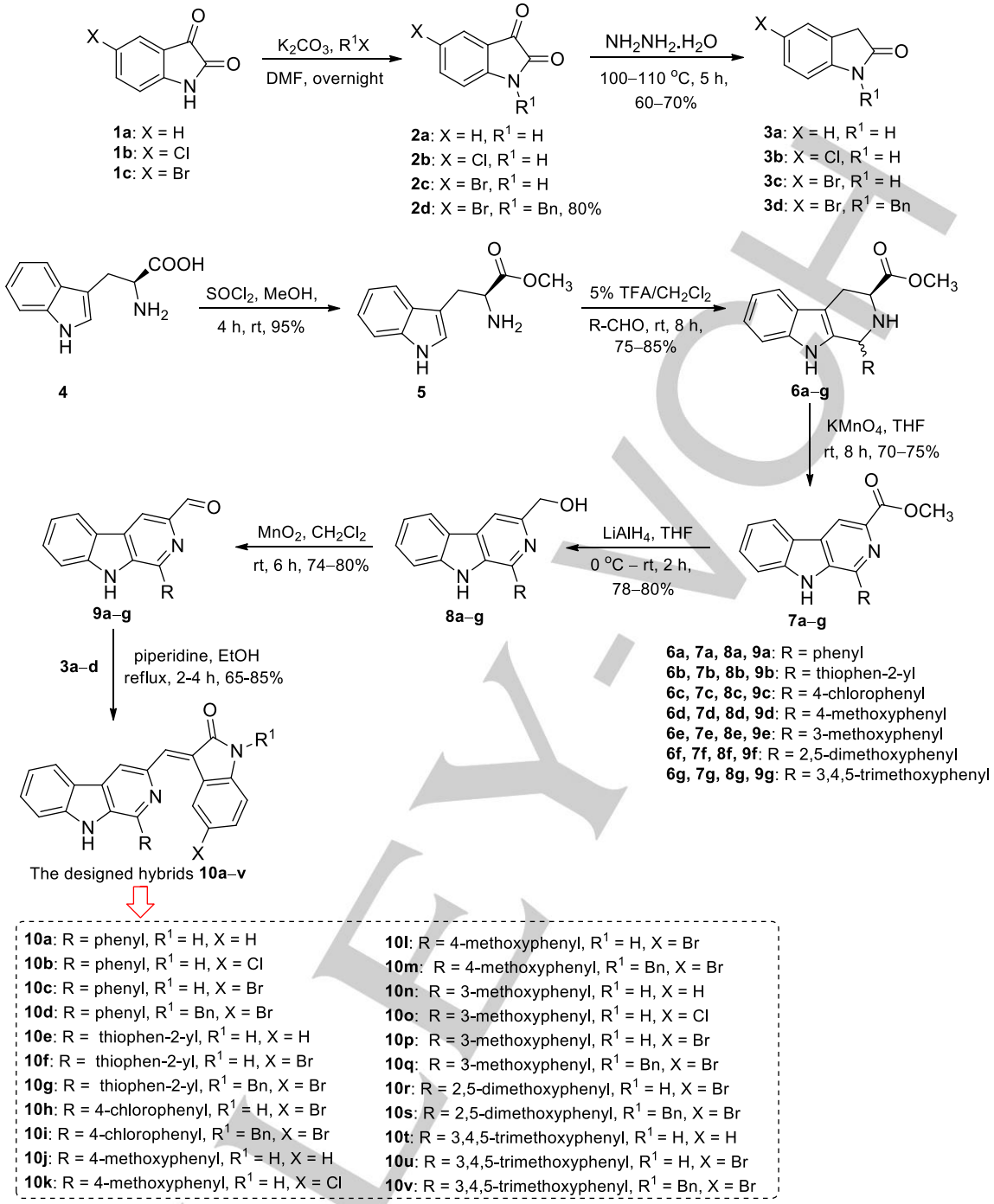

Scheme 1. Design and synthesis of β-carboline linked hybrids **10a**–**v**.

The HRMS (ESI) showed the characteristic protonated $[M + H]^+$ peak to their corresponding molecular formula. To determine the obtained isomer, one of the hybrids **10b** was subjected to NOE experiments. The proton NMR obtained was assigned by gDQFCOSY (see ESI). The presence of NOEs between H5-H6 and H4-H12 suggested that the isomer obtained correspond to *E*-configuration (**Figure 3**).

In vitro cytotoxic activity

The newly synthesized hybrids **10a**–**v** were evaluated for their *in vitro* cytotoxic activity against a panel of human cancer cell lines namely HCT-15, HCT-116, A549, NCI-H460, MCF-7 and a normal lung fibroblasts (HFL-1) cell lines by employing the 3-(4,5-dimethylthiazol-2-yl)-2,5-diphenyltetrazolium bromide (MTT) assay. The results from the *in vitro* anticancer studies revealed that the compounds exhibited diverse anticancer properties and are inferred in **Table 1**. Notably, these compounds exhibited good to moderate cytotoxicity in the tested cancer cell lines. From the close analysis of the IC_{50} values, it was observed that compound **10s** was more significant in inducing cytotoxicity on all the cancer cells and found to be most potent against HCT-15 colon cancer cell line with IC_{50} value 1.43 ± 0.26 μM whereas in A549 lung cancer cell line 50% inhibition was observed at 2.50 ± 0.06 μM. This compound was also found to be active in breast

Table 1. IC_{50} (μM) values[a] against human cancer cell lines by derivatives**10a-v** by MTT assay

Compound	HCT-15[b]	HCT-116[c]	A549[d]	NCI-H460[e]	MCF-7[f]	HFL-1[g]
10a	> 50	42.11±5.62	35.13±4.71	31.21±4.50	45.41±3.51	-
10b	4.80±0.24	10.32±0.72	6.78±0.20	12.86±0.1	14.62±0.58	27.29±4.20
10c	3.12±0.19	9.11±0.21	9.21±0.51	9.10±0.40	9.19±0.07	31.04±5.83
10d	45.80±7.32	48.27±8.65	37.78±3.91	37.10±4.91	33.26±5.54	-
10e	> 50	43.60±5.80	44.12±3.32	33.65±4.81	> 50	-
10f	47.33±4.64	37.65±6.38	48.57±4.12	> 50	44.45±3.81	-
10g	47.12±5.62	38.43±6.12	49.76±1.92	47.21±23.6	35.64±2.21	-
10h	35.23±2.81	48.11±9.28	37.21±2.31	33.42±4.53	35.46±3.62	-
10i	42.25±4.56	31.89±6.21	39.13±4.43	40.26±5.57	44.22±2.25	-
10j	31.25±0.25	34.28±0.35	>50	31.98±0.78	36.84±0.78	-
10k	2.58±0.02	9.39±0.17	10.97±0.46	8.47±0.03	12.05±1.27	34.45±4.21
10l	32.87±0.12	36.85±0.48	34.21±0.56	33.82±0.85	38.12±0.32	-
10m	39.57±4.91	41.67±9.32	41.26±1.56	45.78±3.34	48.18±4.55	-
10n	35.21±0.21	>50	37.12±0.67	34.20±0.12	38.74±0.45	-
10o	36.24±0.48	32.84±0.79	31.97±0.74	35.41±0.78	32.21±0.22	-
10p	30.12±0.41	33.51±0.53	37.58±0.46	36.71±0.76	35.85±0.82	-
10q	38.90±0.05	36.21±0.72	34.41±0.24	32.21±0.87	31.98±1.28	-
10r	39.32±5.27	32.58±3.92	36.46±3.38	34.87±3.53	39.84±5.91	-
10s	1.43±0.26	4.18±0.16	2.50±0.06	6.71±0.2	3.36±0.08	49.79±1.17
10t	48.57±13.27	47.67±9.48	41.45±3.32	41.78±1.74	48.12±3.53	-
10u	18.72±0.12	21.16±0.60	14.46±1.07	29.76±0.50	33.83±2.76	30.30±6.94
10v	> 50	43.48±4.91	40.12±3.64	37.78±0.71	44.65±2.24	-
Harmine [h]	37.91±8.02	31.88±1.16	20.84±3.41	45.41±3.6	46.25±1.43	43.61±2.88
Sunitinib [h]	1.38±0.20	2.18±0.15	1.24±0.11	3.57±0.32	-	-

[a] 50% Inhibitory concentration after 72 h of drug treatment, [b,c] Human colon cancer, [d,e] Human lung cancer , [f] Human breast cancer, [g] Human normal lung fibroblasts, [h] Reference compound. All the values are expressed as Mean ± SEM in which each treatment was performed in triplicate wells.

cancer MCF-7 cell line with an IC_{50} value of 3.36 ± 0.08 μM as compared to the standard compound harmine. Interestingly, the compound **10s** exhibited the least toxicity on normal HFL-1 cell line with IC_{50} value 49.79±1.17 μM. This indicates that the compound **10s** was selective towards the cancer cells rather than normal cell lines tested as represented in **Figure 4**. While the compound **10k** also displayed remarkable cytotoxicity with an IC_{50} value of 2.58 ± 0.02 μM against the colon cancer cell line HCT-15. Among the series tested, the compounds **10b** and **10c** also showed considerable cytotoxicity in all the cancer cell lines.

It is evident from the IC_{50} values (**Table 1**) that C1 position of the β-carboline displayed better cytotoxic activity with different phenyl substitutions (**10b**, **10c**, **10k**, **10s**, and **10u**) rather than the substitutions with heterocyclic entities (**10e**–**10g**). C-5 substituted hybrids (X = Cl or Br) were found to be potent than unsubstituted (X = H) derivatives **10a**, **10e**, **10j**, **10n**, and **10t**. Compound **10s**, with dimethoxy phenyl at C-1 position of β-carboline and N-benzylated, a bromine at C-5 position of oxindole proved to be potent among all the hybrids evaluated. With respect to promising *in vitro* cytotoxicity results (**Table 1**), the significant activity of newly synthesized hybrids **10a**–**v** could also be attributed towards C1 modification of β-carboline by varying different aromatic/heterocyclics in contrast with harmine which bears a methyl group at this position. These biological results could suggest a shore up in anticancer studies that may lead to the discovery of new cytotoxic agents with better activity.

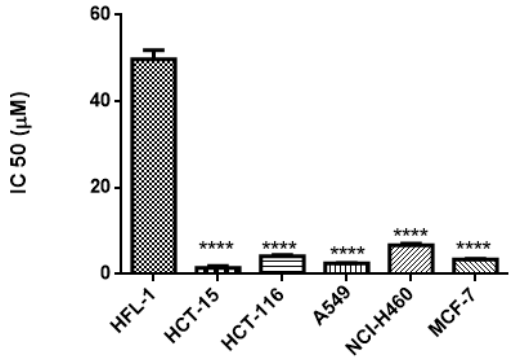

Figure 4. Cytospecificity of compound **10s** towards cancer cells compared to normal fibroblasts HFL-1. Data was expressed as mean ± S.E.M. (n = 3). ****p<0.0001 versus normal cell line.

In vitro growth inhibitory activity

The potent compounds from cytotoxicity studies of **10b**, **10c**, **10k**, **10s**, and **10u** were further assessed for their growth inhibitory potential in human cancer cell lines and a normal cell line by MTT assay. The GI_{50} (μM) values (concentration required to inhibit 50% growth of cancer cells) of the tested compounds were listed in **Table 2**. It is noticeable from the results that some of the compounds have shown moderate to potent growth inhibition against the tested cancer cell lines. Among the series, compound **10s** was found to be the most potent with considerable cell growth inhibition with GI_{50} values of 0.89 ± 0.06 μM in HCT-15 cell lines and found to be efficacious than the parent molecule harmine with GI_{50} of 18.92 ± 4.55 μM. Also, the compound **10s** was found to be effective towards the lung (A549) and breast (MCF-7) cancer cells with significant GI_{50} values of 1.24 ± 0.16, and 1.77 ± 0.17μM, respectively. This compound effectively discriminated the normal and cancer cells by showing minimal toxicity towards the normal lung fibroblast cell line with GI_{50} value 49.4 ± 0.39 μM, approximately 50 fold difference was observed to be an on par with HCT-15 colon cancer cell line. Furthermore, the other derivatives tested among this series for potential cell growth inhibition, the compounds **10c**, **10k**, displayed compelling growth inhibitory activity in colon cancer HCT-15 cells indicating the promising and preferential specificity towards the colon cancer. In addition, the compounds

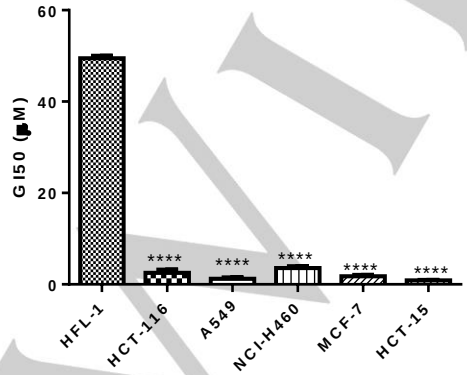

Figure 5. Growth inhibitory potential of compound **10s** towards cancer cells compared to normal fibroblasts HFL-1. Data was represented as mean ± S.E.M. (n=3) ****p<0.0001 versus normal cell line.

10k and **10u** were also efficacious in all the tested cancer cell lines. The remaining compounds were found to be moderately active in growth inhibition of cancer cells. In overall comparison to the standard compound harmine, approximately 20 fold growth inhibitory effects were observed with the compound **10s** against the HCT-15 cell line (**Figure 5**). Hence, the compound **10s** was further selected for mechanistic studies to disclose the mechanism of cell growth inhibition at the molecular level in HCT-15 cell lines. These results may offer a holdup and demonstrated promising evidence in the treatment of cancer that may lead to the breakthrough of identifying novel agents in inhibiting the proliferation of cancer cells.

Apoptosis detection studies

Morphological observations using phase contrast microscope

The induction of apoptotic bodies' formation has always been an ultimate choice in developing anti-cancer therapeutics.[30] To scrutinize whether the treatment with the most active compound **10s** may lead to the induction of apoptosis, HCT-15 cells were treated with the compound **10s**. After 72 h of incubation, images were captured in phase contrast microscope which depicted the loss of cell–cell adhesion, cell wall deformation, shrinkage of cells and resulted in decreased number of viable cells with increased concentration, whereas these characteristic morphological features were lacking in control cells as shown in **Figure 6**.

Acridine orange/ethidium bromide (AO/EB) staining

Acridine orange/ethidium bromide (AO/EB) staining assay was carried out to distinguish between live, apoptotic and necrotic cells. AO can pervade the intact cell membrane and stain the nuclei green, whereas EB can only stain the nuclei of cells that have lost membrane integrity. It can be inferred from **Figure 7** that the control cells exhibited normal morphology and appeared green in color. Whereas the compound **10s** treated cells clearly unveiled the morphological changes such as cell shrinkage, membrane blebbing, chromatin condensation and apoptotic body formation, dose–dependently implying that the compound had prompted apoptosis in HCT-15 cells.

DAPI nucleic acid staining

DAPI (4',6-diamidino-2-phenylindole) is a fluorescent dye that binds sturdily to the nucleus and distinguishes the nuclear damage or chromatin condensation. The DAPI stains the apoptotic cells where apoptotic nuclei appear bright colored due to the condensed nucleus which is a typical apoptotic characteristic. Therefore, to detect nuclear damage or chromatin condensation induced by the compound **10s** in the HCT-15 cell line, DAPI staining technique was performed in compliance with previously reported method.[22] From the results, it was noticed that the nuclear structure of untreated control cells was intact, whereas with the treatment the compound had induced apoptosis with the advent of nuclear changes like condensed,

horse-shoe shaped, pyknotic or fragmented bright nuclei from 0.25 to 2.5 µM concentrations (**Figure 8**).

Table 2. *In vitro* growth inhibitory concentration (GI_{50} µM) [a] against human cancer cell lines by MTT assay

Compound	HCT-15[b]	HCT-116 [c]	A549 [d]	NCI-H460 [e]	MCF-7 [f]	HFL-1 [g]
10b	1.63±0.19	7.66±0.7	4.05±0.13	7.38±1.9	7.47±0.21	18.02±1.62
10c	1.64±0.06	7.94±0.2	6.53±0.22	6.51±0.29	1.66±0.11	17.80±1.51
10k	1.62±0.01	8.52±0.17	8.10±0.20	3.38±0.21	6.05±0.20	26.97±4.34
10s	0.89±0.06	2.52±0.38	1.24±0.16	3.55±0.23	1.77±0.17	49.4±0.39
10u	10.14±2.36	16.46±1.0	7.08±0.61	10.52±0.82	19.0±3.72	19.8±3.51
Harmine[h]	18.92±4.55	23.80±1.5	10.48±0.17	35.91±0.86	20.6±2.47	28.1±2.24
Sunitinib	0.77±0.05	ND	0.52±0.08	0.84±0.14	0.51±0.08	ND

[a] 50% Growth concentration after 72 h of drug treatment, [b,c] Human colon cancer, [d,e] Human lung cancer, [f] Human breast cancer, [g] Human normal lung fibroblasts, [h] Reference compound. All the values are expressed as Mean ± SEM in which each treatment was performed in triplicate wells.

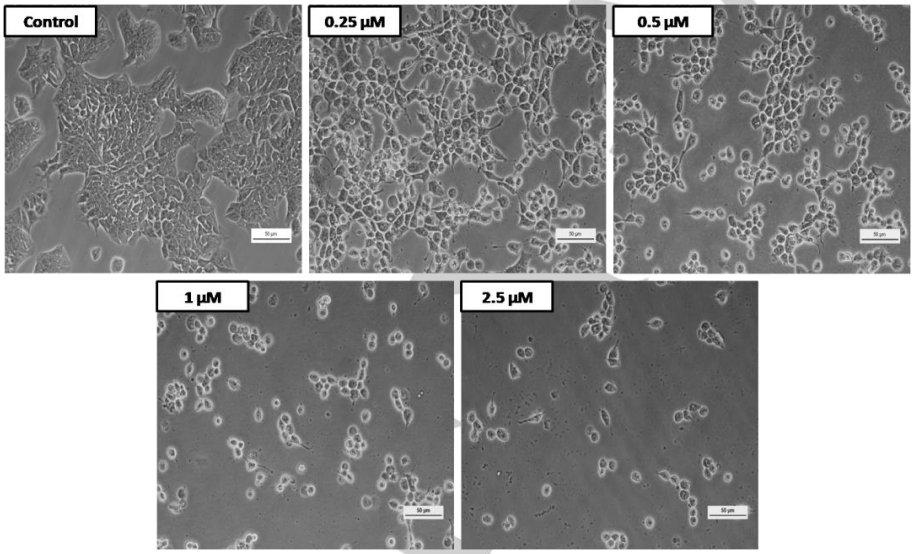

Figure 6. Morphological changes observed in colon cancer cells (HCT-15), cells were treated with and without compound **10s** at concentrations 0.25, 0.5,1, 2.5 µM. After 72 h the images were captured with a phase contrast microscope at 200X magnification.

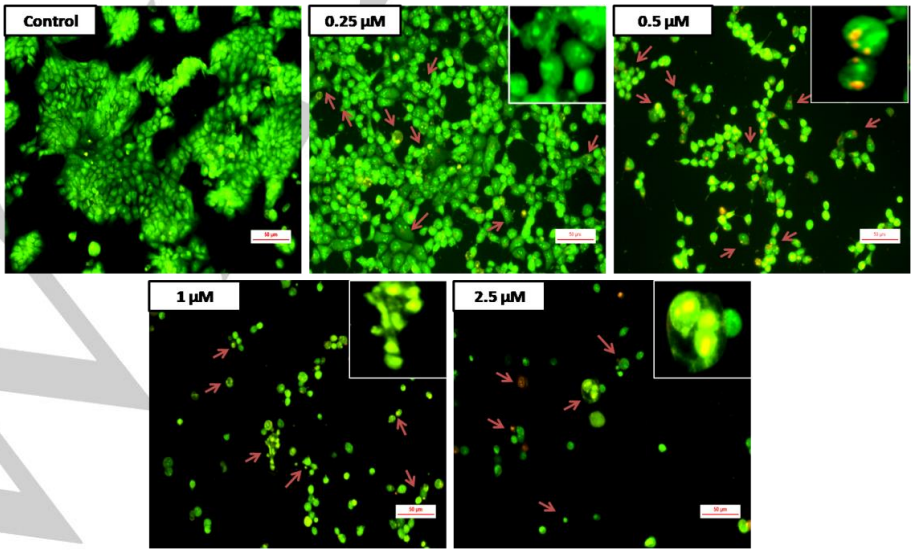

Figure 7. AO/EB staining in colon cancer cell line HCT-15, cells treated with and without compound **10s** at various concentrations 0.25, 0.5, 1 and 2.5 µM for 72 h and compared with control. The images were captured with fluorescence microscope at 200X.

Effect on ROS generation

The excess ROS generation induces irreversible oxidative modification of cellular macromolecules which include lipid, protein or DNA, which disrupt the intracellular redox homeostasis and could lead to apoptotic cell death.[31] Hence, to determine if a pre-treatment with compound **10s** could affect the ROS generation the intracellular ROS levels were determined by using the fluorescent dye DCFDA, which is readily oxidized to 2',7'-dichlorofluorescein (DCF) in the presence of ROS. In our results, the compound **10s** induced the significant generation of ROS dose–dependently as compared to control cells, which exhibited a fruitful avenue for further apoptotic studies (**Figure 9**). The bar diagram also clearly demonstrated the significant induction of ROS levels in **10s** treated cells compared to untreated control cells.

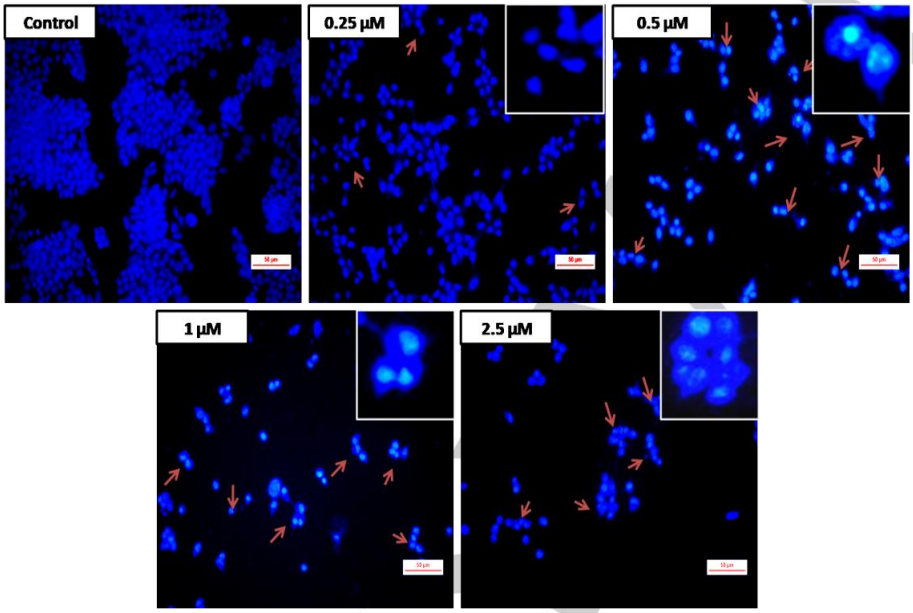

Figure 8. Nuclear morphology of cancer cells after DAPI staining. HCT-15 cells treated with and without compound **10s** at various concentrations 0.25, 0.5, 1 and 2.5 µM for 72 h and compared with control. The images were captured with fluorescence microscope at 200X.

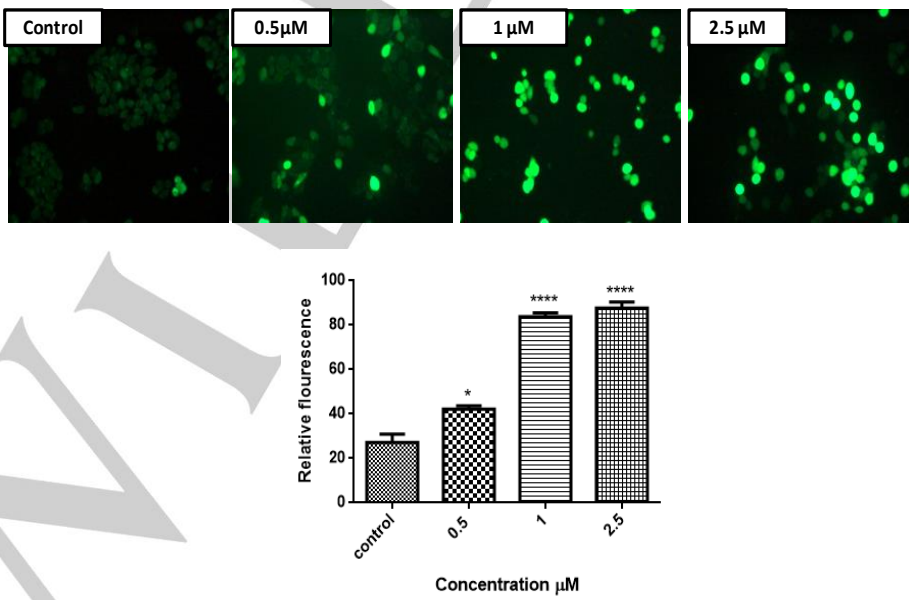

Figure 9. DCFDA staining in colon cancer cell line HCT-15, cells treated with and without compound **10s** at various concentrations 0.5, 1 and 2.5 µM for 72 h and compared with control cells. The images were captured with fluorescence microscope at 200X. The relative DCF fluorescence quantification from the above cells.

Clonogenic assay

The clonogenic assay manifested the effect of compound **10s** on the colony-forming capacity of exponentially growing HCT-15 cancer cells. The results evidenced that the treatment inhibits colony formation potential in the HCT-15 cell population in a concentration–dependent manner. After treatment with various concentrations (0.25, 0.5, 1µM), we observed the formation of colonies in one week time whereas in treatment ascertained clear reduction in the number of colonies as shown in **Figure 10**. Hence, these results specify the significance of compound **10s** in inhibiting the colony formation potential. The total colonies were counted by a molecular imaging system (Vilber Fusion Fx software) and the values were represented as a percent colony forming ability.

Flow-cytometry analysis

Effect on mitochondrial membrane potential ($\Delta\Psi_m$)

The mitochondria play a fundamental task in initiating the intrinsic pathway of apoptosis as it is the foremost target of cellular oxidative stress, which impedes the electron transport chain, leading to reactive oxygen species (ROS) generation and collapse of mitochondrial membrane potential ($\Delta\Psi_m$).[32] Therefore, to appraise the impact of compound **10s** on mitochondria, the $\Delta\Psi_M$ was measured. Treatment of HCT-15 cells with compound **10s** caused a noteworthy reduction in the $\Delta\Psi_m$ compared to control cells as shown in **Figure 11**. The compound **10s** triggered the depolarization of $\Delta\Psi_m$ dose-dependently compared to the control which is illustrating the fatal effects of the compound on mitochondria, thereby assisting the later events of apoptosis.

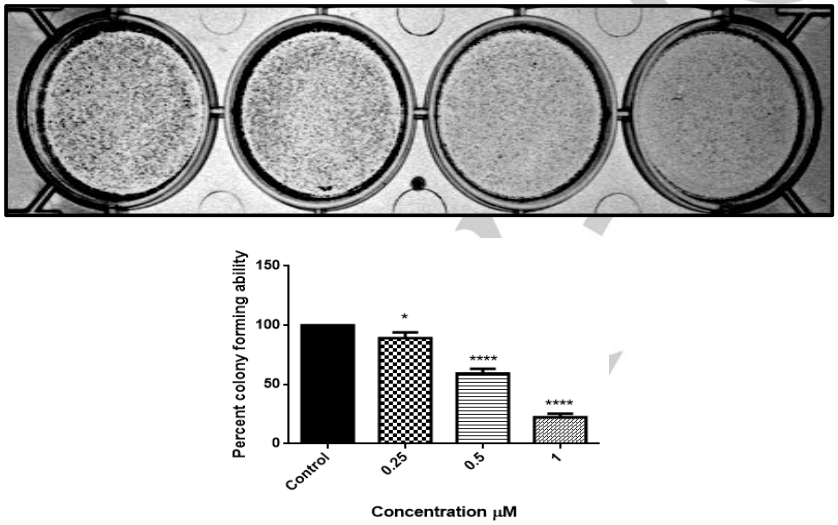

Figure 10. Effect of compound **10s** on colony forming ability of exponentially growing colon cancer cells by clonogenic assay. HCT-15 cells were treated with compound **10s** at 0.25, 0.5,1 µM and allowed to form colonies in fresh medium for 7 days. The images were captured and the colonies were counted with vilber fusion chemdoc imaging system.

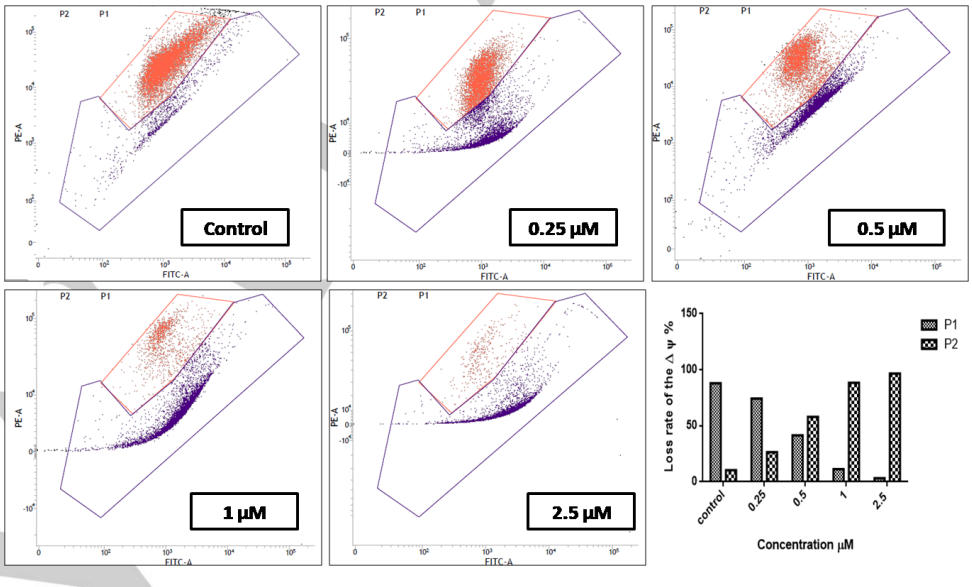

Figure 11. Effect on mitochondrial membrane potential. HCT-15 cells were treated with various concentrations of compound **10s** for 72 h and JC-1 staining was performed. The control represents the cells without compound **10s** treatment.

Cell cycle analysis

From the *in vitro* screening results, it was apparent that the compound **10s** showed significant cytotoxicity against colon cancer HCT-15 cell lines. Hence, in order to disclose whether this cytotoxicity may be due to the cell cycle arrest, analysis of cell cycle was performed. Cells were treated with compound **10s** at concentrations ranging from 0.25 to 2.5 μM for 48 h, and then the cells were stained with propidium iodide and further analyzed by using BD FACSVerse™ flow analyzer. The results from **Figure 12** indicated that the HCT-15 untreated control cells showed 68.71% cells in G0/G1 phase, whereas compound **10s** treatment resulted in elevation in G0/G1 population from 68.7% to 80.61% which gradually subsided with increasing doses. The G0/G1 phase arrest was distinctive at 1 and 2.5 μM concentrations.

Annexin V-FITC/PI assay

Annexin V-FITC/PI dual staining assay was performed using flow cytometry to quantify the apoptotic cell death. HCT-15 colon cancer cells were treated with compound **10s** at different concentrations of 0.25, 0.5, 1.0 and 2.5 μM for 72 h. Results from **Figure 13** indicated the percentage of apoptotic cells and inferred to the significant early and slight late apoptosis induction (Annexin V positive/PI negative) at both 1.0 and 2.5 μM concentration in comparison to control.

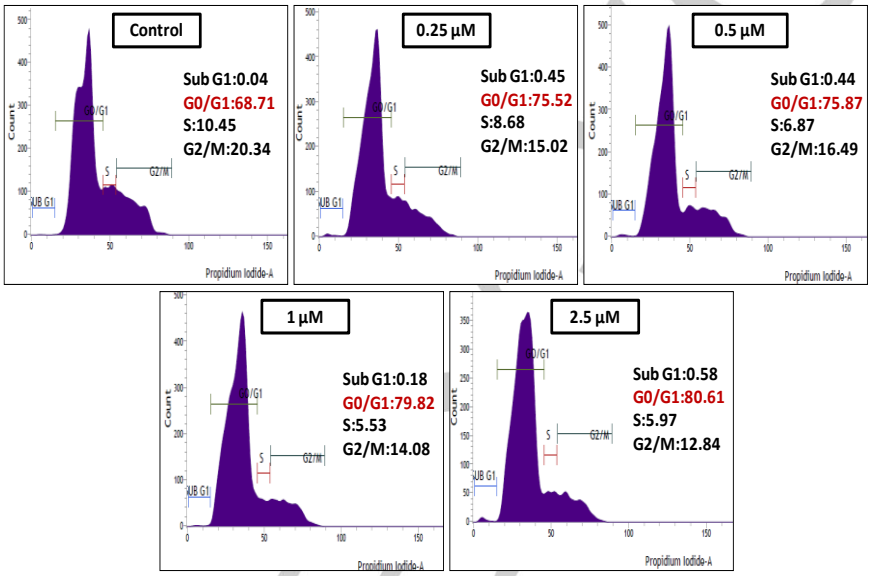

Figure 12. Effect of **10s** on cell cycle progression of colon cancer cells. HCT-15 cells were treated with compound **10s** at 0.25, 0.5, 1, 2.5 μM concentration and cell cycle analysis was performed after 48 h. The analysis of cell cycle distribution was performed by using propidium iodide staining method.

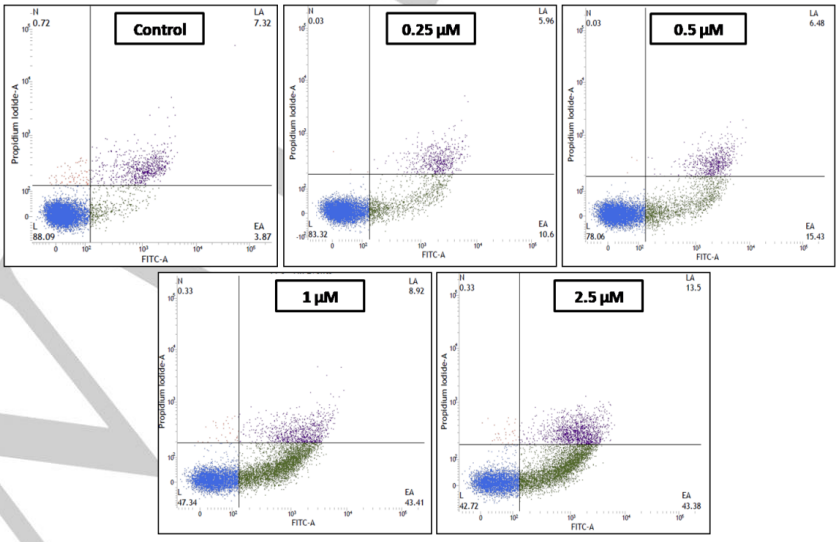

Figure 13. Effect of compound on cell apoptosis as measured by Annexin V-FITC/propidium iodide staining assay. HCT-15 cells were treated with compound **10s** ranging from 0.25 to 2.5 μM concentration for 72 h. Then 10,000 cells from each sample were analyzed by flow cytometry. The percentage of cells positive for Annexin V-FITC and/or Propidium iodide is represented inside the quadrants. Cells in the upper left quadrant (Q1-UL; AV–/PI+): necrotic cells; lower left quadrant (Q2-LL; AV–/PI–): live cells; lower right quadrant (Q3-LR; AV+/PI–): early apoptotic cells and upper right quadrant (Q4- UR; AV+/PI +): late apoptotic cells.

Western blotting

We quested for the molecular mechanisms of apoptosis induction in colon cancer cells. Hence, we assessed the regulation of intrinsic apoptosis accompanied by Bcl-2, Bax, cleaved caspase-3, and 9 proteins, which are intricated in the mitochondrial apoptosis pathway, thus triggers the caspase-dependent apoptotic response. Results from the **Figure 14** stipulated that compound **10s** treatment led to the dose-dependent elevated expression of Bax and cleaved caspase-3, 9 in HCT-15 cells; hence we also corroborated the effect of compound **10s** on the extrinsic apoptotic pathway. As a result, we found increased expression of cleaved caspase-8, which is a key protease, executes apoptosis by cleaving PARP[33] and consistent clear increase in the expression of PARP along with caspase-8. Thus the compound **10s** treatment prompted the activation of both intrinsic and extrinsic pathway.[34]

Molecular docking studies

Most of the β-carboline derivatives were reported to show their action by interacting into DNA.[9] Therefore, to signify the interactions of the synthesized ligands towards DNA and to denote the mode of interaction, molecular modeling studies were performed on DNA hexamer d(CGATCG) using XP Glide[35] (Schrödinger, 2017) with default settings. The docked pose of the compound **10s** was depicted in **Figure 15**, which demonstrates the intercalation of planar β-carboline moiety towards GC base pairs of DNA and C1 substituent aligns at right angles and assists intercalation. The oxindole moiety orients itself perfectly in between GC base pairs. It is also strongly assisted by strong π-π stacking interactions of β-carboline towards dG_6, dG_8, dC_7 residue, along with additional π-cation interactions of nitrogen on C ring of β-carboline with dG_6. Beyond this, benzylated oxindole moiety also shows strong π-π stacking interactions with dC_5. These interactions also well matched with co-crystal structure indicating the intercalation into the DNA.

In order to study the stability of the DNA-ligand complex, Molecular Dynamics (MD) simulations were performed for the best-scored pose of compound **10s** for 20 ns. The images of **10s**-DNA complex throughout the 20 ns MD simulation have shown in **Figure 16**. The plot of root-mean-square deviation (RMSD) of the backbone atoms as a function of time was depicted (**Figure 2**, **ESI**). From the plot, it can be contemplated that the complex does not show major deviation from the initial position over the time period of 20 ns MD simulation. Even the docked pose of **10s** was reasonably stable up to 20 ns MD simulation. The results obtained from molecular simulation studies were compatible with *in vitro* cytotoxicity and relative viscosity results.

Relative viscosity studies

Relative viscosity experiments furnish the confirmation of interaction of newly synthesized hybrids with DNA. Changes in viscosity due to interactions of compounds with DNA can be measured. Intercalation of a compound into DNA results in the increase in relative viscosity due to enhancement in the axial length of DNA helix to naturalize the hybrid. EtBr is a classical measured DNA intercalator which corresponds to the increase in viscosity.[36] Covalent binding to DNA ends up in the decrease in relative viscosity values whereas no; or little change is observed in case of groove binding.[17] Hoechst 33258 is a well-known groove binder and does not affect the relative viscosity

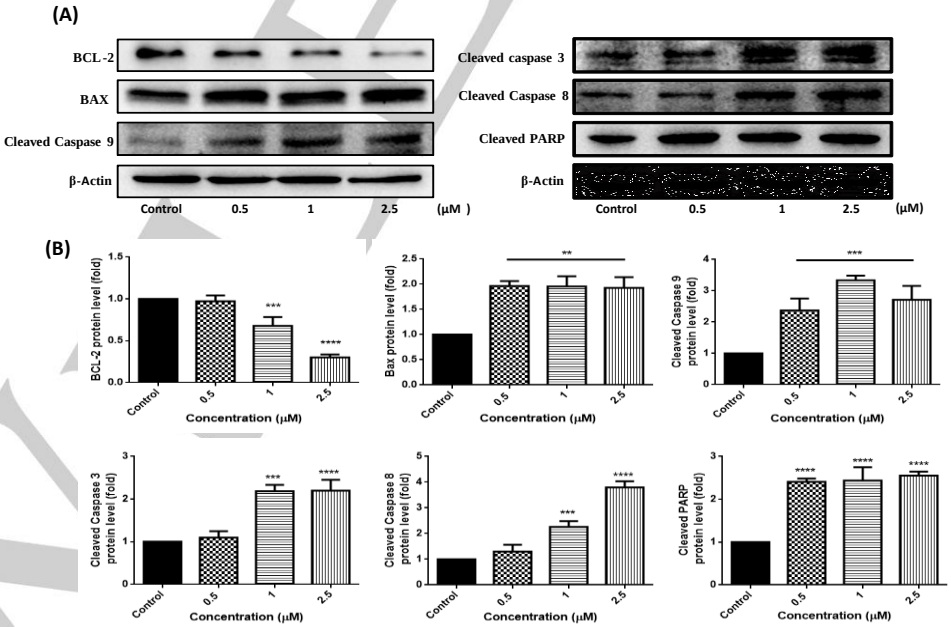

Figure 14. Effect on apoptotic protein expression in HCT-15 cells. Cells were treated with compound **10s** for 48 h and then harvested. Total cell lysates were prepared and 30 μg proteins was subjected to SDS-PAGE followed by western blot analysis and analysed by chemiluminescence detection. (**A**) Western blotting analysis of Bcl-2, Bax, and cleaved caspase-9, 3, 8 and cleaved PARP (**B**) Bar graphs representing the fold changes in the protein expression compared to control. Data expressed as mean ± SEM (n=3). **P<0.01 and ***P < 0.001, ***P < 0.0001 significant vs. control. Band intensities were quantified using NIH Image J software. The western blots shown here are representative of three independent experiments with similar results.

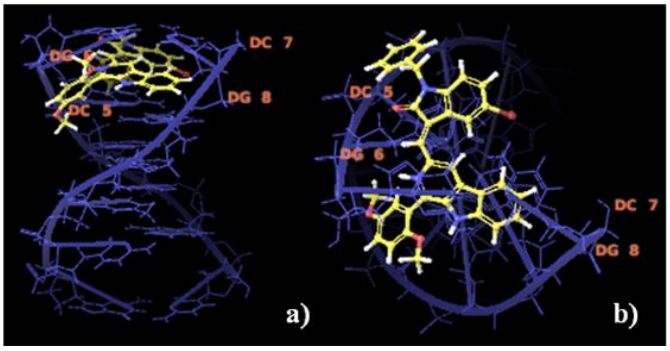

Figure 15. Intercalation of compound **10s** into d(CGATCG). **a**) Side view; **b**) Top view **10s** showing residual interactions with G-C base pairs of DNA. DNA is represented as tube and compound **10s** is represented in yellow color.

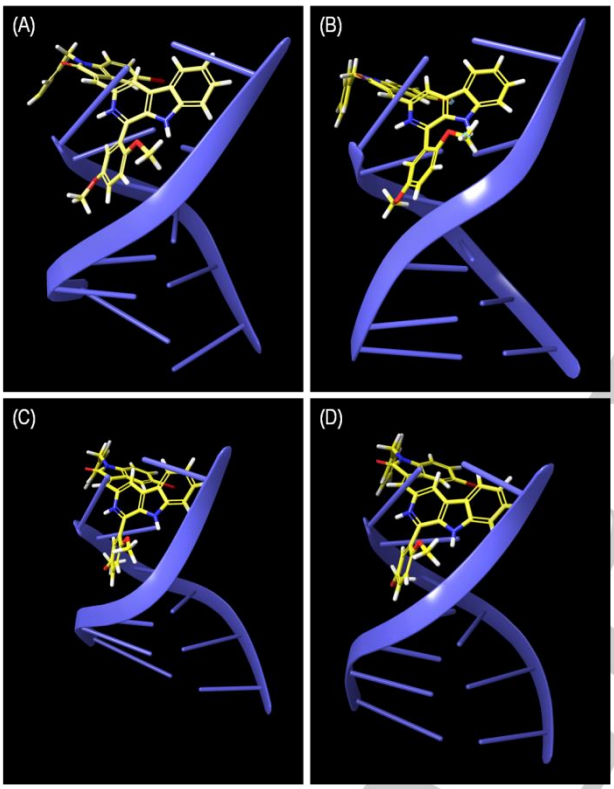

Figure 16. Snapshots **10s**-DNA complex at 5 ns (**A**), 10 ns (**B**), 15 ns (**C**) and 20 ns (**D**) timescale.

when bound to DNA.[37] Addition of compounds **10s** and **10k** results in the increase in viscosity in comparison to the control in concentration-dependent manner, thereby accounting for the DNA intercalation as shown in **Figure 17**. The graph is plotted between concentration (compound/CT-DNA) and viscosity $((\eta/\eta o)^{1/3}$ on X and Y axis respectively with harmine, EtBr and Hoechst 33258 as standards. The viscosity results are consistent with molecular modeling studies.

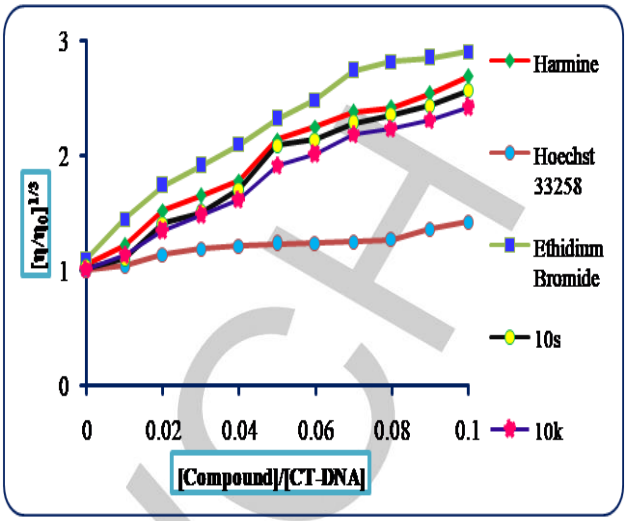

Figure 17. Graphical representation of relative viscosity studies using compound **10s** and **10k** with Harmine, Hoechst-33258, and Ethidium Bromide as reference standards.

Conclusion

In conclusion, a new series of β-carboline-linked oxindole hybrids have been successfully synthesized and evaluated for their *in vitro* cytotoxic potential against a panel of selected cancer cell lines and a normal human cell line. The results of prefatory screening using MTT assay suggests that most of the compounds showed cytotoxic potential at a concentration less than 50 µM. Interestingly, compound **10s** has produced notable cytotoxicity among all the tested cell lines and found to be potent on HCT-15 (colon cancer) cell line with an IC_{50} value of 1.43 ± 0.26 µM. The GI_{50} values also suggest the compound **10s** is potent in comparison to other compounds with a value of 0.89 ± 0.06 µM. The staining studies using AO/EB, DAPI revealed the events of apoptosis and elevated generation of reactive oxygen species (ROS) was indicated by DCFDA staining. Colony formation in HCT-15 was inhibited by compound **10s** in a concentration-dependent manner. Moreover, the flow cytometric studies using compound **10s** in HCT-15 cell line in a dose-dependent manner gave the following observations, i) Cells were arrested at the G0/G1 phase of cell cycle. ii) Annexin V-FITC/PI studies confirmed the significant early and late apoptosis. iii) The collapse of mitochondrial membrane potential ($\Delta\Psi_M$) was evidenced. Further, western-blotting analysis indicated elevated expression of caspase-3, 8, 9, cleaved PARP, Bax, and decrease in levels of Bcl-2 which clearly indicate expression of apoptosis-related proteins. DNA viscosity and molecular modeling studies indicate the intercalation into DNA base pairs. Principally, compound **10s** showed specificity towards the cancer cell line in a cell viability assay in comparison to normal fibroblasts HFL-1 cells. Overall, these current studies imply that these new hybrids have the potential to be developed as lead molecules and suitable structural modifications may ensue in promising anticancer agents.

Experimental Section

Chemistry

General. All reagents and solvents were obtained from commercial suppliers and were used without further purification. Analytical thin layer chromatography (TLC) was performed on MERCK precoated silica gel 60-F_{254} (0.5 mm) aluminum plates. Visualization of the spots on TLC plates was achieved by UV light. ^{1}H and ^{13}C NMR spectra were recorded on Bruker 500 MHz by making a solution of samples in the $CDCl_3$ solvent (or) DMSO using tetramethyl silane (TMS) as the internal standard. Chemical shifts for ^{1}H and ^{13}C are reported in parts per million (ppm) downfield from tetra methyl silane. Spin multiplicities are described as s (singlet), brs (broad singlet), d (doublet), t (triplet), q (quartet), and m (multiplet). Coupling constant (*J*) values are reported in hertz (Hz). HRMS were determined with Agilent QTOF mass spectrometer 6540 series instrument. Wherever required, column chromatography was performed using silica gel (60-120). The reactions wherever anhydrous conditions required are carried under nitrogen positive pressure using freshly distilled solvents. All evaporation of solvents was carried out under reduced pressure using rotary evaporator below 45 ºC. Melting points were determined with an electro thermal digital melting point apparatus IA9100 and are uncorrected. The names of all the compounds given in the experimental section were taken from Chem Bio Draw Ultra, Version 12.0.

General procedure for (E)-3-((1-aryl-9H-pyrido[3,4-b]indol-3-yl)methylene)indolin-2-one (10a–v). To a mixture of oxindole (**3a**–**d**, 1 equiv.), 1-aryl-9*H*-pyrido[3,4-*b*]indole-3-carbaldehyde (**9a**–**g**, 1.1 equiv.), in ethanol, catalytic amount of piperdine was added and refluxed at 80 ºC till complete consumption of the starting materials as determined by TLC. The reaction mixture was cooled, precipitate thus formed was filtered, washed using ethanol to yield pure (*E*)-3-((1-aryl-9*H*-pyrido [3,4-*b*]indol-3-yl)methylene)indolin-2-one in moderate to good yields. All the products were obtained by simple filtration.

Characterization of the synthesized compounds. A complete list of compound characterization is available in the supporting information.

Pharmacology

Cell culture. Cancer cell lines such as colon (HCT-116 and HCT-15), lung (NCI-H460, A549), breast (MCF-7) were maintained in RPMI media while normal lung fibroblasts cell line (HFL-1) were maintained in F12k medium supplemented with 10% fetal bovine serum (FBS) stabilized with 1% antibiotic-antimycotic solution (Sigma) cells were maintained in 5% CO_2 and 98% relative humidity at 37 ºC in incubator. When the cells reached up to 80-90% of confluency, they were sub-cultured using 0.25% trypsin/1 mM EDTA solution for further passage. The compounds were dissolved in DMSO to prepare the stock solution of 10 mM. Further dilutions were made accordingly with respective media to get required concentration.

MTT assay. It is a colorimetric assay that measures the reduction of MTT (3-(4,5-dimethylthiazol- 2-yl)-2,5-diphenyl tetrazolium bromide) to insoluble formazon by mitochondrial succinate dehydrogenase enzyme. Since reduction of MTT can only happen in metabolically active cells, the level of activity is the measure of the viability of the cells.[38] Briefly, cells were seeded in 96-well plates at a density of 1000 to 4000 cells per well in 100 µl of complete medium and allowed to grow overnight for attachment onto the wells. Then the cells were treated with various concentrations of the compounds for a period of 72 h. For cell growth inhibition analysis after 24 h of cell seeding, before treatment (day 0), absorbance was measured by adding MTT in few wells. After 72 h incubation, 100 µl of MTT (0.5 mg/ml) was added and incubated at 37 ºC for 4 h. Then MTT reagent was aspirated and the formazan crystals formed were dissolved by the addition of 200 µL of DMSO for 20 min. at 37 ºC. The formazon product quantity was measured by using a spectrophotometric microtiter plate reader (Spectra Max, M4 Molecular devices, USA) at 570 nM wavelength. The day 0 absorbance was subtracted from the 72 h plates for determining growth inhibition and data were plotted as a percentage of untreated control.

Morphological observations. HCT-15 cells were plated in 12 well culture plates with a cell density of $1x10^5$ cells/mL and allowed to adhere for overnight.[39] The cells were incubated with the 0.25, 0.5, 1, 2.5 µM concentrations of the compound **10s**. After 72 h treatment, cells were observed for the morphological changes and photographs were taken under a phase contrast microscope (Nikon, Inc. Japan).

Acridine orange ethidium bromide (AO/EB) staining. HCT-15 cells were plated at a concentration of $1x10^6$ cells/ml and treated with different concentrations of compound **10s** and the plates were incubated for 72 h. 10 µl of fluorescent dyes containing Acridine Orange (AO) and Ethidium Bromide (EB) were added into each well in equal volumes (10 µg/ml) respectively then the cells were visualized immediately under fluorescence microscope (Nikon, Inc. Japan) with excitation (488 nM) and emission (550 nM) at 200x magnification.

DAPI nucleic acid staining. Morphological changes in nucleus were observed through DAPI staining. After treatment with compound **10s** for 72 h, colon cancer cell line HCT-15 cells were washed with PBS and permeabilized with 0.1% Tween 20 for 10 min followed by staining with 1 µM DAPI. Control and treated cells were observed with fluorescence microscope with excitation at 359 nM and emission at 461 nM using DAPI filter at 200x magnification.

DCFDA staining. DCFDA staining was performed to determine the reactive oxygen species (ROS) levels as per reported method[37] with slight modifications. For this experiment, HCT-15 cells were plated at cell density of 3.5×10^5 cells/well into 12-well plates in RPMI supplemented with 10% FBS. Then the cells were treated with the compound **10s** at various concentrations for 72 h. Then the DCFDA reagent was added at 10 µM concentration for 15 min and the fluorescent intensity was captured using fluorescent microscope at 200X magnification. The relative DCF fluorescence in the cells was measured by spectramax.

Clonogenic growth inhibition assay. Colon cancer cells HCT-15 were passaged in RPMI 1640 supplemented with 10% fetal bovine serum on at 37 ºC in an atmosphere containing 5% CO_2. Exponentially growing cells were seeded into 12-well culture plates and kept overnight and treated with the compound **10s**. Every 3 days the medium was removed and replaced with fresh medium. After 7 days of incubation, the colonies were fixed and stained with 1% crystal violet in methanol for 3 h. The number of stained colonies were counted under chemdoc imaging system (Vilber Fusion Fx, France).Colony formation was calculated as a percentage to untreated control cultures.[40]

Flow cytometric analysis

Measurement of mitochondrial membrane potential. HCT-15 cells ($1x10^6$ cells/ml) were seeded in 12 well plates and allowed to adhere for overnight. The cells were incubated with compound **10s** at 0.25, 0.5, 1 and 2.5 µM concentrations for 48 h. Cells were collected and washed with PBS and resuspended in solution of JC-1 (1 µM) and incubated for 30 min in incubator at 37 ºC. The cells were washed twice with PBS and analysed by flow cytometer (BD FACSVerse™, USA).

Cell cycle analysis. Flow cytometric analysis (FACS) was performed to calculate the distribution of the cell population in various cell cycle phases. In general the novel compounds exert their cytotoxic or growth inhibitory effect by arresting the specific checkpoint in cell cycle.[41] Here HCT-15 cancer cells were incubated with compound **10s** at various

concentrations from 0.25 to 2.5 µM for 24 h. Untreated and treated cells were harvested, washed and fixed overnight in 70% ethanol in PBS at -20 ºC. Fixed cells were pelleted and stained with cell cycle analysis reagent propidium iodide (50 µg/ml) with RNase A for 20 min at 37 ºC in dark according to the manufacturer instructions and about 10,000 events were acquired and analyzed on a flow cytometer BD FACSVerse™ (BD Biosciences, USA).

Annexin V assay. It was performed by the method given by Rieger *et al*. with slight modifications.[42] Briefly, 1 X 10^5 cells were seeded in a 12-well plate and treated with different concentration of compound **10s** for 72 h. Then Untreated and treated cells were harvested and the cells were processed with Annexin V-FITC and Propidium Iodide (PI) staining (BioLegend) according to the manufacturer's instructions. Further, flow cytometric analysis was performed using a flow cytometer (BD FACSVerseTM, USA). Apoptosis and necrosis were analyzed with quadrant statistics on propidium iodide-negative cells, fluorescein positive cells and propidium iodide (PI)-positive cells, respectively.

Western blotting. After treatment with various concentrations of compound **10s** in HCT-15 cells for 48 h cells were washed twice in 1X PBS, then lysed with RIPA buffer which includes protease and phosphatase inhibitors and incubated on ice for 40 min. Cell lysates were then centrifuged for 15 min at 13,000 rpm at 4 ºC and the supernatant was collected. Protein concentration was determined by bicinchoninic acid method. Equal amounts of protein were separated using SDS–PAGE and subsequently transferred to nitrocellulose membrane by using a trans-blot system (Transblot SD: Semidry transfer cell; Bio-Rad Laboratories) The blots were blocked with 3% BSA in TBS-T (20 mM Tris– HCl, pH 7.4, 137 mM NaCl, and 0.05 %Tween-20) at room temperature for 2 h and incubated overnight with the relevant primary antibody. Immunoreactivity was detected using either an anti-mouse or anti-rabbit peroxidase-conjugated secondary IgG antibody for 1 hour. To ensure equal loading of protein β-actin was used as an internal control. Bands were monitored using enhanced chemiluminescence reagent (Millipore, U.S.A). under chemdoc imaging system (Vilber Fusion Fx, France).The strength of western blotting bands was determined by Image J density measurement program.

Molecular docking studies. The DNA crystal structure has been retrieved from Protein Data Bank (PDB ID: 1NAB).[43] The preparation of the DNA hexamer was performed using Protein preparation tool. This adds up the missing atoms and removes peripheral water molecules with a distance of more than 3 Å from the pocket. The grid is generated by picking the active site where the co-crystal is located and grid box of 10 × 10 × 10 Å was generated using Glide 7.4 (Schrödinger 2017-1).[35] The potent hybrid was sketched (**10s**) by using 2D sketcher and energy minimized and subjected to ligand preparation for generation of different conformers (Schrödinger 2017-1). The different conformers thus generated were subjected to molecular docking with SP Glide 7.4 (Schrödinger 2017-1). The poses thus generated were evaluated and best one was reported. The lowest energy pose for the compound was selected and the docked complex were further optimized using molecular dynamics simulations using Desmond 4.4 with OPLS-AA force field in explicit solvent with the TIP3P water model. Before MD simulations, the systems were minimized and pre-equilibrated using the default relaxation routine implemented in Desmond. The complexes present in trajectory file after production phase of MD simulations, were clustered according to the RMSD of backbone. The RMSD plot was obtained from simulation event analysis of Desmond.

Relative viscosity studies. Lovis 2000 M/ME Rolling-ball viscometer (Anton Paar GmbH, Graz, Austria) was used to determine the viscosities of the DNA-ligand complexes, based on the falling ball principle. The temperature at ±0.005 K was controlled by means of an internal Peltier thermostat. A calibrated 1.59 mm glass capillary containing a steel ball was filled with the sample for measuring the ball falling time at angles in the range from 20º to 70º. The kinematic as well as dynamic viscosities were estimated based on the ball falling time at 25 ºC and densities DNA solution was prepared in 100 mM Tris-HCl (pH 7.4) and viscosity was measured while each derivative (5µM) was added to CT-DNA solution (50 µM). Ethidium bromide, Harmine and Hoechst 33258 at 5 µM concentration were used as reference standards. Data was represented graphically as $(\eta/\eta_0)^{1/3}$ vs. the ratio of the concentration of the hybrid to CT-DNA, where η is the viscosity of CT-DNA in the presence of the derivative and η_0 is the viscosity of CT-DNA solution.

Acknowledgments

The authors are thankful to DoP, Ministry of Chemicals & Fertilizers, Govt. of India, for the award of NIPER fellowship and Dr. Gannoju Srinivasulu for his help in the interpretation of NMR and 2D NMR studies. Dr. N. Shankaraiah gratefully acknowledges SERB, DST, Govt. of India for research grant (YSS-2015-001709).

Keywords: β-Carboline • indoline-2-one • cytotoxicity • DNA intercalation • flow cytometry

References:

1. (a) https://www.cancer.gov/about-cancer/understanding/statistics; (b) http://www.who.int/mediacentre/factsheets/fs297/en/
2. R. Siegel, K. D. Miller, A. Jemal, CA, *Cancer J. Clin*. **2017**, *67*, 7-30.
3. (a) L. H. Hurley, *Nat. Rev. Cancer*. **2002,** *2,* 188-200; (b) J. Sheng, J. Gan, Z. Huang, *Med Res Rev*. **2013**, *33*, 1119-1173.
4. S. Nekkanti, R. Tokala, N. Shankaraiah, *Curr. Med. Chem.* **2017,** *24,* 2887-2907.
5. D. Hanahan, R. A. Weinberg, *Cell*, **2011,** *5***,** 646-674.
6. (a) R. A. Abrimovitch, I. D. Spencer, *Adv. Heterocycl. Chem.***1964**, *3,* 79-207; (b) M. Moloudizargari, P. Mikaili, S. Aghajanshajeri, M. H. Asghari, J. Shayegh, *Pharmacogn. Rev.* **2002**,*14*, 199-212; (c) A. Kamal, M. Sathish, A. V. G. Prasanthi, J. Chetna, Y. Tangella, V. Srinivasulu, N. Shankaraiah, A. Alarifi, *RSC Adv.* **2015**, *5*, 90121-90126.
7. (a) H. J. Shin, H. S. Lee, D. S. Lee, *J. Microbiol. Biotechnol*. **2010,** *20***,** 501–505; (b) R. B. Volk, F. H. Furkert, *Microbiol. Res.* **2006,** *161*,180–186; (c) K. L. Rinehart Jr., J. Kobayashi, G. C. Harbour, J. Gilmore, M. Mascal, T. G. Holt, L. S. Shield, F. Lafargue, *J. Am. Chem. Soc.* **1987**, *109*, 3378–3387; (d) K. V. Rao, N. Kasanah, S. Wahyuono, B. L. Tekwani, R. F. Schinazi, M. T. Hamann, *J. Nat. Prod.* **2004**, *67*, 1314–1318; (e) N. Shankaraiah, C. Jadala, S. Nekkanti, K. R. Senwar, N. Nagesh, S. Shrivastava, V. G. M. Naidu, M. Sathish, A. Kamal, *Bioorg. Chem.* **2016**, *64,* 42-50.
8. R. Cao, W. Peng, Z. Wang, A. Xu, *Curr. Med. Chem*. 2**007,** *14,* 479-500.
9. (a) Z. Chen, R. Cao, L. Yu, B. Shi, J. Sun, L. Guo, Q. Ma, W. Yi, X. Song, H. Song, *Eur. J. Med. Chem.* **2010**, *45,* 4740-4745; (b) N. Shankaraiah, K. P. Siraj, S. Nekkanti, V. Srinivasulu, P. Sharma, K. R. Senwar, M. Sathish, M. V. P. S. Vishnuvardhan, S. Ramakrishna, C. Jadala, N. Nagesh, A. Kamal, *Bioorg. Chem.* **2015,** *59*, 130-139; (c) Z. Chen, R. Cao, B. Shi, W. Yi, L. Yu, H. Song, Z. Ren, W. Peng, *Bioorg. Med. Chem. Lett.* **2010,** *20*, 3876-3879; (d) J. M. Giulietti, P. M. Tate, A. Cai, B. Cho, S. P. Mulcahy, *Bioorg. Med. Chem. Lett.* **2016**, *26*, 4705-4708; (e) N. Shankaraiah, P. Sharma, S. Pedapati, S. Nekkanti, V. Srinivasulu, N. P. Kumar, A. Kamal, *Lett. Drug. Des. Discov.* **2016**, *13*, 335-342.
10. Y. Li, F. Liang, W. Jiang, F. Yu, R. Cao, Q. Ma, X. Dai, J. Jiang, Y. Wang, S. Si, *Cancer Biol. Ther*. **2007,** *6*, 1193–1199.
11. P. A. Barsanti, W. Wang, Z. Ni, D. Duhl, N. Brammeier, E. Martin,. *Bioorg. Med. Chem. Lett*. **2010**, *20*, 157.

12. (a) N. Göckler, G. Jofre, C. Papadopoulos, U. Soppa, F. J. Tejedor, W. Becker, *FEBS J.* **2009**, *276*, 6324–6337; (b) A. Seifert, L. A. Allan, P.R. Clarke, *FEBS J.* **2008**, *275*, 6268–6280.
13. A. C. Castro, L. C. Dang, F. Soucy, L. Grenier, H. Mazdiyasni, M. Hottelet, L. Parent, C. Pien, V. Palombella, J. Adams, *Bioorg. Med. Chem. Lett.* **2003**, *13*, 2419.
14. J. I. Trujillo, M. J. Meyers, D. R. Anderson, S. Hegde, M. W. Mahoney, W. F. Vernier, I. P. Buchler, K. K. Wu, S. Yang, S. J. Hartmann, D. B. Reitz, *Bioorg. Med. Chem. Lett.* **2007**, *17*, 4657-4663.
15. J. Zhang, Y. Li, L. Guo, R. Cao, P. Zhao, W. Jiang, Q. Ma, H. Yi, Z. Li, J. Jiang, J. Wu, Y. Wang, S. Si, *Cancer, Biol. Ther.* **2009**, *8*, 2374–2383.
16. X. Li, B. Bai, L. Liu, P. Ma, L. Kong, J. Yan, J. Zhang, Z. Ye, H. Zhou, B. Mao, H. Zhu, Y. Li, *Cell Death Discov.* **2015**, *1*, 15033-15041.
17. (a) A. Kamal, V. Srinivasulu, V. L. Nayak, M. Sathish, N. Shankaraiah, C. Bagul, N. V. S. Reddy, N. Rangaraj, N. Nagesh, *Chem. Med. Chem.* **2014**, *9*, 2084-2098; (b) J. Jiménez, L. Riverón-Negrete, F. Abdullaev, J. Espinosa-Aguirre, R. Rodríguez-Arnaiz, *Exp. Toxicol. Pathol.* **2008**, *60,* 381- 389; (c) A. Kamal, M. Sathish, V. L. Nayak, V. Srinivasulu, B. Kavitha, Y. Tangella, D. Thummuri, C. Bagul, N. Shankaraiah, N. Nagesh,. *Bioorg. Med. Chem.* **2015**, *23*, 5511-5526; (d) M. Sathish, B. Kavitha, V. L. Nayak, Y. Tangella, A. Ajitha, S. Nekkanti, A. Alarifi, N. Shankaraiah, N. Nagesh, A. Kamal, *Eur. J. Med. Chem.* **2018**, *144*, 557-571.
18. J. Kovvuri, B. Nagaraju, V. L. Nayak, R. Akunuri, M. P. N. Rao, A. Ajitha, N. Nagesh, A. Kamal, *Eur. J. Med. Chem.* **2018**, *143,* 1563-1577.
19. Z. Chen, R. Cao, B. Shi, W. Yi, L. Yu, H. Song, Z. Ren, W. Peng, *Bioorg. Med. Chem. Lett*. **2010**, *20,* 3876-3879.
20. D. Singh, P. Sharma, R. Kumar, S. K. Pandey, C. C. Malakar, V. Singh, *Asian J. Org. Chem*. **2018**, *7*, 6-36.
21. G. Momekov, A. Bakalova, M. Karaivanova, Curr*. Med. Chem.* **2005**, *12*, 2177.
22. P. Sharma, D. Thummuri, T. S. Reddy, K. R. Senwar, V. G. M. Naidu, G. Srinivasulu, S. K. Bhargava, N. Shankaraiah, *Eur. J. Med. Chem.* **2016**, *122*, 584-600.
23. (a) J. Ma, S. Li, K. Reed, P. Guo, J.M. Gallo, *J. Pharmacol. Exp. Ther.* **2003**, *305,* 833–839; (b) M. E. Lane, B. Yu, A. Rice, K. E. Lipson, C. Liang, L. Sun, C. Tang, G. McMahon, R. G. Pestell, S. Wadler,*Cancer Res.* **2001**, *61*, 6170–6177.
24. (a) L. Sun, C. Liang, S. Shirazian, Y. Zhou, T. Miller, J. Cui, J. Y. Fukuda, J. Y. Chu, A. Nematalla, X. Wang, H. Chen, A. Sistla, T. C. Luu, F. Tang, J. Wei, C. Tang, *J. Med. Chem.* **2003**, *46*, 1116-1119; (b) R. Roskoski Jr, *Biochem. Biophys. Res. Commun.* **2007**,*356,* 323-328.
25. (a) A. Kamal, V. S. Reddy, S. Karnewar, S. S. Chourasiya, A. B. Shaik, G. B.Kumar, C. Kishor, M. K. Reddy, M. P. Narasimha Rao, A. Nagabhushana, K. V. Ramakrishna, A. Addlagatta, S. Kotamraju, *Chem. Med. Chem*. **2013**, *8*, 2015-20125; (b) A. Kamal, M. P. N. Rao, P. Das, P. Swapna, S. Polepalli, V. D. Nimbarte, K. Mullagiri, J. Kovvuri, N. Jain, *Chem. Med. Chem*. **2014**, *9*, 1463-1475.
26. C. Viegas-Junior, A. Danuello, V. da Silva Bolzani, E. J. Barreiro, C. A. Fraga, *Curr. Med. Chem*. **2007**, *14*, 1829-1852.
27. L. Sun, N. Tran, F. Tang, H. App, P. Hirth, G. McMahon, C. Tang, *J. Med. Chem*. **1998**, *41***,** 2588–2603.
28. C. Crestini, R. Saladino, *Synth. Commun*. **1994**, *20*, 2835-2841.
29. N. Devi, G. Kaur, D. Singh, S. Mor, V. P. R. K. Putta, S. Polina, C. C. Malakar, V. Singh, *New J. Chem.* **2016**, *41*, 1082-1093.
30. S. Elmore, *Toxicol. Pathol*. **2007**, *35,* 495–516.
31. M. L. Circu, T. Y. Aw, *Free Radic. Biol. Med*. **2010**, *48*, 749–62.
32. J-C Ahn, J-W Kang, J-I Shin, P-S Chung, *Int. J. Oncol*. **2012**, *41*, 2184–90.
33. A. H. Boulares, A. G. Yakovlev, V. Ivanova, B. A. Stoica, G. Wang, S. Iyer, M. Smulson, *J. Biol. Chem*. **1999**, *33*, 22932-30.
34. J. Chen, F. Peng, Y. Zhang, B. Li, J. She, X. Jie, Z. Zou, M. Chen, L. Chen, *Eur. J. Med. Chem*. **2017**,*140*, 104-117.
35. Schrödinger suite **2017**-1; Schrödinger, LLC: New York, **2017**.
36. S. Nekkanti, V. Pooladanda, M. Veldandi, R. Tokala, C. Godugu, N. Shankaraiah, *ChemistrySelect.* **2017**, *2*, 7210–21.
37. S. Nekkanti, K. Veeramani, S. S. Kumari, R. Tokala, N. Shankaraiah, *RSC Adv*. **2016**, *6***,** 103556-103566.
38. A. Subramanian, S. Arunachalam, R. Arun, K. Premkumar, *RSC Adv*. **2013**, *3*, 16456-16468.
39. A. Jain, V. Pooladanda, U. Bulbake, S. Doppalapudi, T. A. Rafeeqi, C. Godugu, W. Khan, Nanomedicine *Nanotechnol. Biol. Med*. **2017**, *13*, 2251–2262.
40. S. J. Moghaddam, P. Barta, S. G. Mirabolfathinejad, Z. Ammar-Aouchiche, N. T. Garza, T. T. Vo, *Carcinogenesis*. **2009**, *11,* 1949–56.
41. M. J. Cecchini, M. Amiri, F. A. Dick, *J. Vis. Exp. JoVE*. **2012**, *59*, e3491-e3497.
42. A. M. Rieger, K. L. Nelson, J. D. Konowalchuk, D. R. Barreda, *J. Vis. Exp.JoVE*. **2011**, *20*, e2597-e2600.
43. C. Temperini., L. Messori., P. Orioli., C. D. Bugno., F. Animati., G. Ughetto, *Nucleic Acids Res*. **2003**, *31*, 1464-1469.

Entry for the Table of Contents

Insert graphic for Table of Contents here. ((Please ensure your graphic is in **one** of following formats))

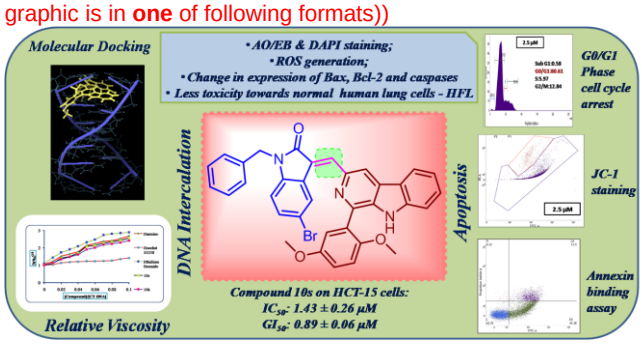

A series of β-carboline linked oxindole derivatives have been synthesized *via* knoevenagel condensation. These new compounds have been evaluated for their *in vitro* cytotoxic activity and DNA intercalation.